Ultrafast laser micromachining of submillimetric de Laval nozzles in alumina for laser electron acceleration

Armando V. F. Zuffi
IPEN – CNEN/SP
São Paulo, SP, Brazil
armandozuffi@gmail.com

Fabio B. D. Tabacow
IPEN – CNEN/SP
São Paulo, SP, Brazil
fabio.tabacow@gmail.com

Nilson D. Vieira Jr.
IPEN – CNEN/SP
São Paulo, SP, Brazil
nilsondiasvieirajr@gmail.com

Ricardo E. Samad
IPEN – CNEN/SP
São Paulo, SP, Brazil
resamad@gmail.com

2022 SBFoton International Optics and Photonics Conference (SBFoton IOPC) | 978-1-6654-5273-1/22/$31.00 ©2022 IEEE | DOI: 10.1109/SBFotonIOPC54450.2022.9992490

***Abstract*—We have explored the fabrication of submillimetric de Laval nozzles by ultrashort laser pulses micromachining in alumina, a dielectric ceramic, to generate supersonic gas jets in vacuum. The nozzles were manufactured in a home-built trepanning setup, and their geometry and surface quality dependence on the laser and machining parameters was investigated, aiming to control the jet spatial density to produce optimal gaseous targets for laser electron acceleration.**

Keywords— ultrafast laser micromachining, laser ablation, de Laval nozzle, supersonic gas target, laser wakefield acceleration.

I. INTRODUCTION

Laser wakefield acceleration (LWFA) has been growing rapidly as a new concept for the next generation of compact electron accelerators [1]. Since this technique can create acceleration gradients over 100 GV/m, a few orders of magnitude higher than those currently in conventional RF accelerators (~100 MV/m) [2, 3], the accelerated electrons can reach up to GeV in a few centimeters [4, 5], consequently reducing the laboratory dimensions as well as its costs. In practice, LWFA usually occurs when high-intensity laser pulses are focused in a gaseous target inside a vacuum environment, creating a plasma region with a periodic charge distribution that originates a longitudinal electric field (wakefield) capable of accelerating electron bunches [6]. In addition to fundamental physics research, LWFA has been addressing a wealth of applications [7], including radioisotope production for nuclear medicine and protontherapy [8, 9]. For this application scope, the generation of electron bunches at repetition rates in the kHz range is required, and it can be achieved using the so-called *self-modulated* LWFA (SM-LWFA) [10, 11]. This technique requires modest tabletop laser systems with pulses of about 100 fs and peak powers of a few TW, which become resonant with a high density plasma wave by the self-modulation process.

In order to generate optimal electron bunches in the SM-LWFA regime (energies up to dozens of MeV, quasi-monoenergetic and low divergence), thin and flat-top gaseous target with well-defined high-densities regions are required [12, 13]. This kind of targets are usually supersonic gas jets generated by de Laval nozzles [13, 14], expanding in a vacuum environment and pulsed synchronously with the laser. The geometry of those converging-diverging nozzles is illustrated in Fig. 1. In this kind of nozzle, a high-pressure gas in the backing chamber originates a flow, which is subsonic in the nozzle converging section, that compresses the gas passing the throat, through the diverging section where the gas axial velocity progressively increases due to a free expansion and after the exit exhausts into the vacuum environment as a supersonic jet [15]. On a first-order approximation and assuming an isotropic flow, the Mach number, M, reached by the gas jet is defined by the ratio between the exit and the throat areas of the de Laval nozzle, according to [16]:

$$A_{ext}/A_{thr} = 1/M\,[2+(\gamma\text{-}1)M^2/\,\gamma+1]^{(\gamma+1)/[2(\gamma-1)]} \qquad (1)$$

where A_{ext} and A_{thr} are the exit and the throat areas, respectively, and γ is the gas heat capacity ratio (adiabatic index). Although the theoretical quasi-1D model that includes (1) presents good agreement with experimental results, this model does not consider other geometrical features such as the nozzle length, the lengths of the converging and diverging sections, their curvatures, and the internal walls roughness; all of these affect the jet profile and speed as second-order corrections [16], being better explored by Computational Fluid Dynamic (CFD) simulations [17].

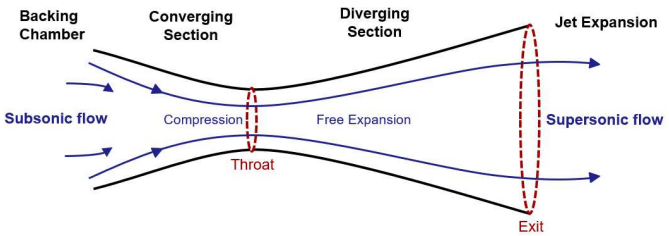

Fig. 1. Scheme of a de Laval nozzle geometry. Blue lines represent the gas flow from the subsonic to the supersonic regime through the converging-diverging sctions of the nozzle.

Our research group is working to implement the first laser electron acceleration infrastructure in Latin America at the Nuclear and Energy Research Institute (IPEN) [18, 19], aiming to produce ^{99}Mo by a gamma-induced nuclear photoreaction from ^{100}Mo driven by SM-LWFA electron bunches [20]. Particle-in-cell (PIC) simulations have been showing us the possibility to generate dozens of MeV electron bunches by SM-LWFA, using TW or sub-TW laser pulses and gaseous targets with submillimetric dimensions [21-23]. Therefore, we have been working on the development of techniques to manufacture submillimetric de Laval nozzles [24, 25], as well as methods to diagnose the

This work was supported by FAPESP, SAE and CNPq grants.

supersonic gas jets created by the manufactured nozzles and the laser-induced-plasma into the gaseous target [24, 26, 27].

Regarding the submillimetric de Laval nozzle manufacture, we have worked on different approaches using ultrashort laser pulses micromachining to fabricate nozzles with exit diameters in the range of 100-300 μm. The ultrafast laser micromachining promotes high precision etching on the micrometric scale due to the non-linear interaction of ultrashort pulses with the matter, producing a non-selective and non-thermal ablation [28-30]. The laser ablation produces diverging holes due to the focused beam converging geometry and the pulses energy losses as the substrate is being etched [30, 31], naturally reproducing a de Laval nozzle geometry.

We initially manufactured de Laval nozzles in metallic substrates using laser micromachining by the percussion method [24, 25]. Nonetheless, this method, in conjunction with the low ablation threshold of metals [32, 33], produced non-circular and asymmetric holes due to inhomogeneities in the intensity profile of the focused laser.

The best results came from micromachining de Laval nozzles on dielectric substrates by trepanning [25, 28, 34], which is proving to be suitable for our proposes. The trepanning method rotates the substrate in which the nozzle is being manufactured, smoothing out the laser beam inhomogeneities and preserving the cylindrical symmetry. Additionally, it allows deeper ablation into the substrate by creating flat surfaces for successive pulses, significantly reducing the loss of energy by reflection at grazing incidence in the etched walls. Also, replacing the metallic substrates by dielectric ones, which have two orders of magnitude higher ablation thresholds [33, 35], makes the ablation less sensitive to laser intensity fluctuations, ensuring a more accurate etching.

We established a methodology to manufacture high-quality submillimetric de Laval nozzles by trepanning using ultrafast laser micromachining on alumina substrates (Al_2O_3), a dielectric ceramic. This strategy has been producing nozzles that originate supersonic jets with interaction lengths of about 100 μm [17, 24, 27], producing optimal gaseous targets for the laser-plasma accelerator. In this work, we present our procedures to fabricate the submillimetric nozzles by ultrafast laser machining in a home-built trepanning setup. In addition, the de Laval nozzle geometry and internal walls roughness dependence on the pulse laser and machining parameters was explored. These outcomes contribute to our goals to establish a laser electron acceleration infrastructure in Brazil based on SM-LWFA.

II. Methodology

A Ti:Sapphire CPA laser system (Femtolasers Femtopower Compact Pro HR/HP) has been used for micromachining the de Laval nozzles. This system produces 25 fs (FWHM) pulses centered at 785 nm with 40 nm of bandwidth (FWHM), up to 650 μJ, operating at 4 kHz repetition rate, and M^2 factor of 1.5. These ultrashort pulses are directed to the machining setup shown in Fig. 2. This arrangement is composed of a rotating DC electric motor coupled to a 3-axis computer-controlled micrometric positioning system (Newport UTS100C stages) mounted in a XYZ configuration. The motor rotates at a 20-30 RPM and its axis is parallel to the laser propagation direction, and an achromatic doublet focuses the laser pulses orthogonally to the surface of the substrate holder. Alumina plates with 0.6 mm thickness are placed in the substrate holder, and when the DC motor rotates, the laser etches a circular hole on the alumina surface by trepanning, and after the appropriate time, the laser trespasses the plate, producing a highly circular de Laval nozzle in it.

As exposed in (1), the most important parameters to define the Mach number of a gas jet are the throat and the exit areas of the nozzle. Due to the nonlinear character of the ablation process, we observed that the throat and the exit diameters depend on the following laser and machining parameters: laser intensity, beamwaist position in the substrate, and exposure time after the nozzle is bored. The laser intensity in the alumina can be controlled by tunning the pulse energy and the doublet focal length. The focal length values explored were 30, 50, 75, 150, and 250 mm. Considering the laser beam diameter at the doublet as 8 mm, we could estimate the focused beamwaist for each focal length, evaluating the laser intensity on the substrate during the ablation process. Furthermore, the beamwaist position in the substrate (at its surfaces, or inside it), regarding confocal volume into the substrate, determines the laser intensity distribution and, consequently, the ablation geometry profile. This parameter is easily controlled by the micrometric positioning system (XYZ translator). Finally, the exposure time is also easily controlled by a shutter that blocks the laser pulses. We observed that increasing the exposure time after the laser trespasses the plate enhances the circularity of the exit and the throat and improves the internal wall roughness.

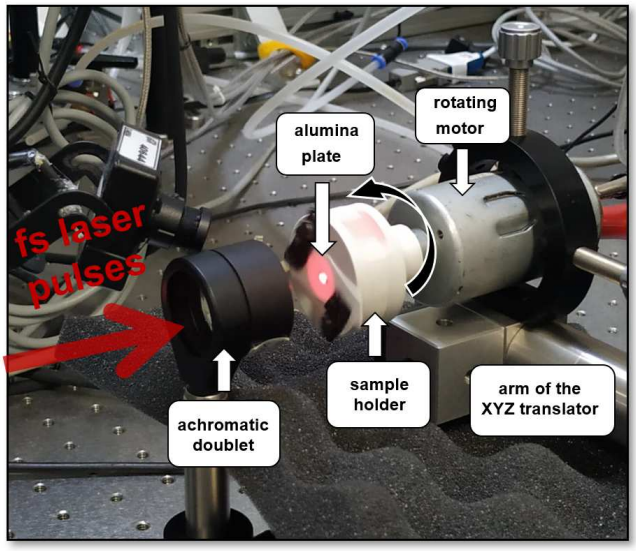

Fig. 2. Ultrafast laser micromachining on an alumina plate fixed to the machining setup (rotating electric motor with substrate holder).

After the de Laval nozzle is etched, the alumina plate is moved laterally by 1 mm, and the laser cuts a 2 mm diameter disk with the nozzle exactly at its center (Fig. 3a). From the alumina disk we can characterize the exit and throat diameters and circularity by optical profilometry (Zegage optical profilometer, Zygo Inc.), and the morphology of the nozzle internal walls by scanning electron microscopy (TM3000, Hitachi Inc). Following these steps, the alumina disk is glued to the tip of a metal part, as shown in Fig. 3b, using a vacuum compatible epoxy glue (Torr Seal) that has a breaking tension above the one exerted in the alumina disk by a pressure of 50 bar. This metal part has a 1 mm hole through it, defining the backing chamber after the tip is connected to the gas line.

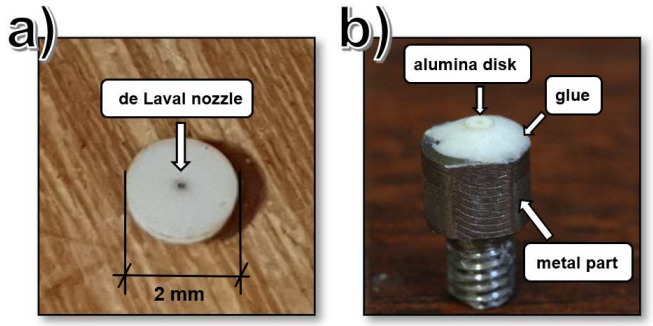

Fig. 3. (a) 2 mm diameter alumina disk with a de Laval nozzle at its center. b) Alumina disk glued to the tip of the metal part to connect to the gas line.

III. RESULTS

We currently have manufactured more than 40 de Laval nozzles exploring the following machining parameters: 1) doublet focal length, 2) beamwaist position in the substrate, 3) laser pulse energy, and 4) exposure time after boring the nozzle. Moreover, we have accumulated experience with other nozzle fabrication processes that were not successful for our purposes, due to reasons such as low intensity that failed to ablate the nozzle in the alumina, big exit diameter (> 500 µm), noncircular hole due to laser misalignments with the rotation axis of the machining setup, among others.

The nozzles produced by this manufacturing approach typically have high cylindrical symmetry, demonstrating the high quality and precision of the trepanning machining process, allied to the use of alumina. Fig. 4 shows profilometries of the exit (135 µm diameter) and throat (45 µm diameter) of a typical submillimetric nozzle, resulting in an estimated Mach number of ~4.8 when using He (γ=1.66) in (1). The machining parameters for this nozzle fabrication were 480 µJ pulses focused by the 75 mm focal length doublet, and an exposure time of 15 s after boring the nozzle. During this manufacture, the beamwaist was initially placed in the center of the alumina plate, and during the ablation process it was progressively moved to the plate back-face to increase the throat diameter. We observed that the throat enlargement provides a higher gas flow, suitable to our proposes. However, the drawback is the decrease of the Mach number.

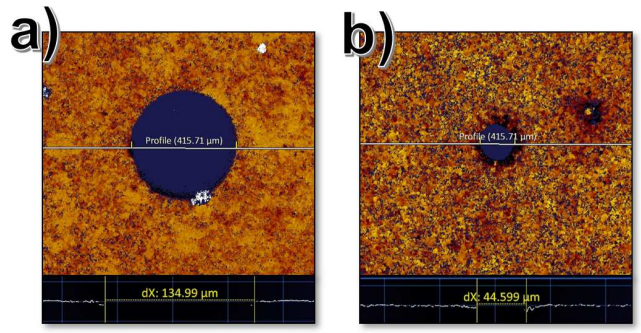

Fig. 4. Submilimetric de Laval nozzle profilometry. (a) 135 µm nozzle exit diameter. (b) 45 µm nozzle throat diameter.

Fig. 5 exhibits scanning electron micrographies (SEM) of another nozzle showing its exit and throat, with of 170 µm and 30 µm diameters, respectively (both visible in Fig. 5a). This de Laval nozzle was manufactured by 400 µJ pulses, a 30 mm focal length doublet, beamwaist position in the center of the alumina plate, and exposure time of 30 s. Despite some debris inside the nozzle that can be easily removed, the nozzle internal walls are very smooth, with smaller roughness than that of the alumina surface, which is clearly observed in the exit nozzle edge exhibited with a higher magnification in Fig. 5b. Those characteristics indicate a change in the alumina structure during the ablation process due to the melting and ressolidification of the ceramic grains [25, 36, 37], consequence of residual heat due to elevated pulse energy and high repetition rate. The ressolidification fuses the alumina grains [38] and produce the low roughness, smooth walls, which should decrease turbulences in the gas jet.

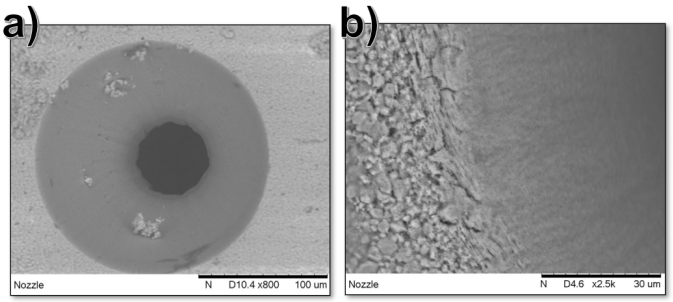

Fig. 5. SEM of de Laval nozzle with 170 µm exit and 30 µm throat diameters. (a) view of the entire nozzle. (b) detail of the exit nozzle edge, highlighting its smooth walls with smaller roughness than the alumina surface.

Regarding the machining dependence on the achromatic doublet focal length, we observed that the best results were obtained with f = 75 mm, and that it comes from the tradeoff between the required laser intensity to bore the 0.6 mm thick plate and the confocal volume into that plate. Due to the energy loss during the machining process (grazing incidence) we estimated that intensities above 3×10^{14} W/cm^2 are needed to bore the alumina plate, therefore smaller focal length doublets (30, 50 and 75 mm) are more suitable for etching the substrate since they can exceed this intensity. However, the shorter lenses create smaller confocal parameters, of about 0.1 mm (f = 30 mm) and 0.3 mm (f = 50 mm), which are under than half of the alumina plate thickness. Therefore, when using these doublets, the beamwaist should be placed at the center of the plate to reach a condition to bore it, and small pointing fluctuations of the laser can impair the manufacture. The 75 mm doublet produces a ~0.6 mm confocal parameter, close to the alumina thickness, allowing more reproducibility and different beamwaist positions for the manufacture. We even manufactured nozzles with 150 mm and 250 mm focal length doublets, but the reproducibility was not good, and the time to bore the nozzle could surpass 1 hour due to the smaller intensities.

Due to the previously estimated intensity to bore the alumina plates, we observed that the laser pulse energies to manufacture the nozzle depend on the focal length used. For the 75 mm doublet, the best results (smaller nozzle exit and throat diameters, high circularity and smooth walls) were obtained using ~400 µJ. For the 30 mm doublets the energy was closer to 300 µJ, and for longer focal lengths (150 mm) more than 500 µJ were needed.

We also observed that when the beamwaist is positioned at the alumina surface (nozzle exit surface – processing laser entrance), due to the energy losses during the ablation, the laser hardly bored the alumina plate. Moving the beamwaist to the plate back-surface (nozzle throat surface – processing laser exit), an increasing of the exit and throat diameters was

obtained, producing, normally, exit diameters bigger than the desired values (>200 µm). The smallest diameters were produced when the beamwaist was positioned at the center of the alumina plate, resulting in the best energy distribution inside the substrate. However, we observed that the jets generated by the nozzles exhibited smaller Mach numbers than estimated theoretical by (1). The reason for this comes from the curvature of the nozzle diverging section that, in second order approximation, defines the jet Mach number. Fig. 6 presents a SEM of the cross section of a de Laval nozzle cleaved along its length. This nozzle was fabricated with the beamwaist positioned in the center of the alumina plate. The nozzle has the shape of a convex trumpet, the curvature that presents the smaller Mach number [39] for a given ratio between the throat and exit diameters. Recently, we started to manufacture de Laval nozzles initially positioning the beamwaist at the center of the plate, and quickly moving it to the nozzle throat surface, as done in the nozzle exhibited in Fig. 4. We believe that this approach can change the nozzle shape to a concave bell, the curvature with the higher Mach number [39].

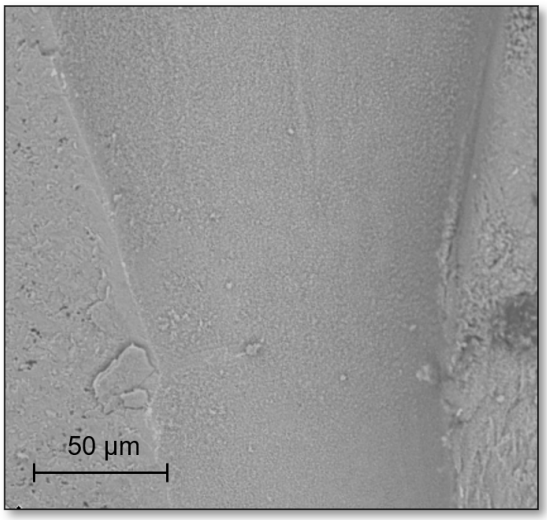

Fig. 6. SEM micrography of the transversal profile of a de Laval nozzle manufactured with the beamwaist at the center of the alumina plate, evidencing a convex trumpet profile.

The last machining parameter explored was the exposure time after boring the nozzle. We observed that this time is critical to improve the smoothness in the nozzle walls resulting from the melting and ressolidification process. In order to create very smooth walls with low roughness, times above 10 s are necessary for the typical machining parameter used. Fig. 7 shows two manufactured nozzles with similar exit and throat diameters (~160 µm and ~40 µm) and similar machining parameters (f = 30 mm, ~400 µJ, and beamwaist positioned at the center of the alumina plate), except for the exposure time after boring the nozzle. In Fig. 7a this exposure time was 30 s, and in Fig. 7b it was only 3 s. For the smaller time, the walls present periodic structures created by the trepanning process, which were not completely smoothed by the melting and ressolidification due the lower exposure time and deposited energy. We believe that the residual heat necessary for the melt and ressolidification is more present after the nozzle is bored, since the energy transfer from the plasma to the alumina becomes more frequently, increasing the melting and the surface tension that smooths the surface before the ressolidification occurs.

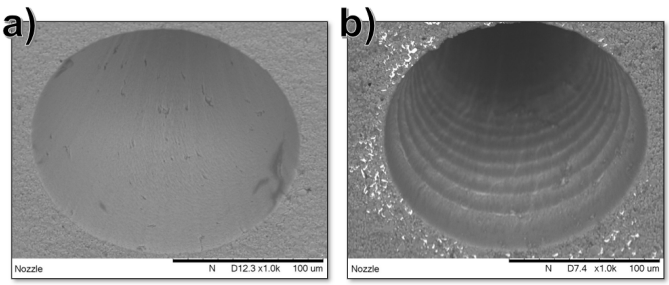

Fig. 7. SEM micrographies of nozzles manufactured with a) a long (30 s) and b) a short (3 s) exposure time after boring the noozle.

Finally, Fig. 8 exhibits a high Mach number helium gas jet target created in vacuum by a nozzle with a 300 µm diameter exit and a 150 µm diameter throat. Laser pulses are hitting the target close to the nozzle, creating a plasma, and the excited atoms leave the laser interaction region at supersonic speeds, revealing the jet shape as they decay and emit light.

Fig. 8. Helium gas jet produced by a de Laval nozzle in vacuum, exhibiting a plasma excited by ultrashort pulses. The jet shape can be observed by the light emitted by He moving at supersonic speeds out of the laser interaction region.

IV. Conclusions

We were successful in developing a method to manufacture submillimetric de Laval nozzles for electron laser acceleration by micromachining alumina by trepanning with ultrashort laser pulses. The nozzles manufactured exhibit throats and exits with high circularity and smooth internal walls, which should decrease turbulence in the jet targets created.

Changing the machining parameters, we could control the nozzle throat and exit diameters, which are the primary characteristics that define the jet Mach number. We are working to improve the control of the nozzle shape, which introduces second order corrections on the targets density profiles, which are important for the electrons acceleration dynamics.

Acknowledgment

The authors would like to acknowledge the financial support from FAPESP (grants 2018/25961-7 and 17/50332-0), SAE and CNPq (scholarship to Zuffi and grant 465763/2014-6).

References

[1] T. Katsouleas, "Accelerator physics - Electrons hang ten on laser wake," Nature, vol. 431, pp. 515-516, 2004.

[2] V. Malka, "Laser plasma accelerators," Phys. Plasmas, vol. 19, 2012.

[3] V. Malka, "Plasma Wake Accelerators: Introduction and Historical Overview," Cern Yellow Rep., vol. vol. CERN-2016-, pp. 1–28, 2016.

[4] W. P. Leemans, "GeV electron beams from a centimetre-scale accelerator," Nat. Phys., vol. 2, pp. 696-699, 2006.

[5] A. J. Gonsalves, "Petawatt Laser Guiding and Electron Beam Acceleration to 8 GeV in a Laser-Heated Capillary Discharge Waveguide," Phys. Rev. Lett., vol. 122, 2019.

[6] E. Esarey, C. B. Schroeder, and W. P. Leemans, "Physics of laser-driven plasma-based electron accelerators," Rev. Mod. Phys., vol. 81, pp. 1229-1285, 2009.

[7] F. Albert, "Laser Wakefield Accelerators: Next-Generation Light Sources," Optics and Photonics News, pp. 42-49, 2018.

[8] F. Kroll, "Tumour irradiation in mice with a laser-accelerated proton beam," Nat. Phys., vol. 18, pp. 316-+, 2022.

[9] K. Nemoto, "Laser-triggered ion acceleration and table top isotope production," Appl. Phys. Lett., vol. 78, pp. 595-597, 2001.

[10] A. J. Goers, "Multi-MeV Electron Acceleration by Subterawatt Laser Pulses," Phys. Rev. Lett., vol. 115, 2015.

[11] F. Salehi, "MeV electron acceleration at 1 kHz with <10 mJ laser pulses," Opt. Lett., vol. 42, pp. 215-218, 2017.

[12] B. Hidding, "Quasimonoenergetic electron acceleration in the self-modulated laser wakefield regime," Phys. Plasmas, vol. 16, 2009.

[13] J. Faure, "A review of recent progress on laser-plasma acceleration at kHz repetition rate," Plasma Phys Contr F, vol. 61, 2019.

[14] K. Schmid, and L. Veisz, "Supersonic gas jets for laser-plasma experiments," Rev. Sci. Instrum., vol. 83, 2012.

[15] K. Foelsch, "The Analytical Design of an Axially Symmetric Laval Nozzle for a Parallel and Uniform Jet," J Aeronaut Sci, vol. 16, pp. 161-&, 1949.

[16] F. Sylla, Veltcheva, S. Kahaly, A. Flacco, and V. Malka, "Development and characterization of very dense submillimetric gas jets for laser-plasma interaction," Rev. Sci. Instrum., vol. 83, p. 033507, 2012.

[17] F. B. D. Tabacow, A. V. F. Zuffi, E. P. Maldonado, and R. E. Samad, Vieira, N.D., "Theoretical and experimental study of supersonic gas jet targets for laser wakefield acceleration," in *2021 SBFoton International Optics and Photonics Conference (SBFoton IOPC)*, 2021, pp. 1-5.

[18] N. D. V. Junior, "Laser particle acceleration in Brazil," presented at the 2019 International Nuclear Atlantic Conference - INAC 2019, Santos, Brazil, 2019.

[19] N. D. V. Junior, "Compact Laser Accelerators for medical applications," presented at the XLIV Congress of the Brazilian Biophysical Society, Santos, Brazil, 2019.

[20] N. D. Vieira, "Laser wakefield electron accelerator: possible use for radioisotope production," in *2021 SBFoton International Optics and Photonics Conference (SBFoton IOPC)*, 2021, pp. 1-5.

[21] E. P. Maldonado, R. E. Samad, A. V. F. Zuffi, F. B. D. Tabacow, and N. D. Vieira, "Self-modulated laser-plasma acceleration in a H2 gas target, simulated in a spectral particle-in-cell algorithm: wakefield and electron bunch properties," in *2019 SBFoton International Optics and Photonics Conference (SBFoton IOPC)*, São Paulo, Brazil, 2019, p. 5.

[22] E. P. Maldonado, "Electron beam properties in self-modulated laser wakefield acceleration using TW and sub-TW pulses," in *2021 SBFoton International Optics and Photonics Conference (SBFoton IOPC)*, 2021, pp. 1-5.

[23] E. P. Maldonado, "Study of quasimonoenergetic electron bunch generation in self-modulated laser wakefield acceleration using TW or sub-TW ultrashort laser pulses," Aip Adv, vol. 11, p. 065116, 2021.

[24] R. E. Samad, A. V. F. Zuffi, E. P. Maldonado, and N. D. Vieira, "Development and Optical Characterization of Supersonic Gas Targets for High-Intensity Laser Plasma Studies," presented at the 2018 SBFoton International Optics and Photonics Conference (SBFoton IOPC), Campinas, Brazil 2018.

[25] B. B. Chiomento, "Development of dielectric de Laval nozzles for laser electron acceleration by ultrashort pulses micromachining," in *2021 SBFoton International Optics and Photonics Conference (SBFoton IOPC)*, 2021, pp. 1-5.

[26] A. V. F. Zuffi, E. P. Maldonado, N. D. Vieira, and R. E. Samad, "Time-Resolved Femtosecond Laser-Plasma Measurements by a Mach-Zehnder-Like Interferometer," in *Latin America Optics and Photonics Conference*, Recife, Brazil, 2022.

[27] A. V. F. Zuffi, E. P. Maldonado, N. D. Vieira, and R. E. Samad, "Development of a modified Mach-Zehnder interferometer for time and space density measurements for laser wakefield acceleration," in *2021 SBFoton International Optics and Photonics Conference (SBFoton IOPC)*, 2021, pp. 1-5.

[28] S. Mishra, and V. Yadava, "Laser Beam MicroMachining (LBMM) - A review," Opt. and Las. in Eng., vol. 73, pp. 89-122, 2015.

[29] M. P. Raele, L. R. De Pretto, W. de Rossi, N. D. Vieira, and R. E. Samad, "Focus Tracking System for Femtosecond Laser Machining using Low Coherence Interferometry," Sci. Rep., vol. 9, 2019.

[30] J. Cheng, "A review of ultrafast laser materials micromachining," Opt. Laser Technol., vol. 46, pp. 88-102, 2013.

[31] A. V. Lugovskoy, and I. Bray, "Ultrafast electron dynamics in metals under laser irradiation," Phys. Rev. B, vol. 60, pp. 3279-3288, 1999.

[32] S. Nolte, "Ablation of metals by ultrashort laser pulses," J. Opt. Soc. Am. B, vol. 14, pp. 2716-2722, 1997.

[33] R. E. Samad, L. M. Machado, d. R. W., and N. D. Vieira, Ultrashort Laser Pulses Machining: InTech, 2012.

[34] A. Tuennermann, S. Nolte, and J. Limpert, "Femtosecond vs. Picosecond Laser Material Processing," Laser Technik Journal, vol. 7, pp. 34-38, 2010.

[35] M. D. Perry, "Ultrashort-pulse laser machining of dielectric materials," J. Appl. Phys., vol. 85, pp. 6803-6810, 1999.

[36] M. Garcia-Lechuga, J. Solis, and J. Siegel, "Melt front propagation in dielectrics upon femtosecond laser irradiation: Formation dynamics of a heat-affected layer," Appl. Phys. Lett., vol. 108, 2016.

[37] Q. T. Le, C. Bertrand, and R. Vilar, "Femtosecond laser ablation of enamel," J Biomed Opt, vol. 21, 2016.

[38] B. Nie, H. Huang, S. Bai, and J. Liu, "Femtosecond laser melting and resolidifying of high-temperature powder materials," Appl. Phys. A-Mat. Sci. Proc., vol. 118, pp. 37-41, 2015.